

# Stark localization as a resource for weak-field sensing with super-Heisenberg precision

Xingjian He,<sup>1,\*</sup> Rozhin Yousefjani,<sup>1,†</sup> and Abolfazl Bayat<sup>1,‡</sup>

<sup>1</sup>*Institute of Fundamental and Frontier Sciences, University of Electronic Science and Technology of China, Chengdu 610051, China*

Gradient fields can effectively suppress particle tunneling in a lattice and localize the wave function of a single particle at all energy scales, a phenomenon known as Stark localization. The energy-dependent Stark localization transition point, i.e. mobility edge, tends to a transition at infinitesimal fields as the system size increases, closely resembling the Anderson localization without disorder. Here, we show that the single-particle Stark probe not only achieves quantum-enhanced sensitivity for weak-field sensing but also allows for strong super-Heisenberg scaling across its entire spectrum. This quantum-enhanced sensitivity, which is well-beyond most of the known quantum sensing schemes, stretches from the extended phase and goes beyond the transition point and can be achieved by a simple position measurement. Moreover, through extensive finite-size scaling analysis, we have identified several critical exponents of the Stark localization transition and established their relationship. Interestingly, at finite temperatures, the achievable precision reduces to Heisenberg scaling, which is still well beyond the capability of classical sensors. We have also identified a universal behavior for Stark probes at thermal equilibrium with respect to their temperature and system size.

*Introduction.*— Cramér-Rao inequality lies at the foundation of estimation theory [1–3]. It bounds the precision for estimating an unknown parameter  $h$ , quantified by standard deviation  $\delta h$ , through  $\delta h \geq 1/\sqrt{\mathcal{M}\mathcal{F}}$ , where  $\mathcal{M}$  is the number of samples and  $\mathcal{F}$  is Fisher information. Generally, Fisher information scales with the probe size  $L$  as  $\mathcal{F} \sim L^\beta$ . While classical probes can at best achieve linear scaling, i.e.  $\beta=1$  (standard limit), quantum features may enhance the precision to super-linear scaling with  $\beta>1$  [4–6]. Originally, highly entangled states, known as GHZ states [7], have been used for achieving  $\beta=2$  (Heisenberg limit) [8–16]. However, those schemes are prone to decoherence and are fundamentally limited to Heisenberg scaling (i.e.  $\beta=2$ ). Alternatively, many-body probes can achieve quantum-enhanced sensitivity by harnessing a variety of quantum features. A class of such probes exploits various forms of criticality such as first-order [17–19], second-order [20–34], dissipative [35–41], time crystals [42], and topological [43–46] phase transitions. Other quantum many-body probes rely on quantum scars [47–50] and Floquet driving [51, 52] as well as adaptive [53–62], continuous [41, 63–66], and sequential [67, 68] measurements. There are two key open problems in many-body sensors. First, although the precision of these probes is not fundamentally bounded (i.e. no restriction on  $\beta$ ), it is very hard to find quantum probes whose precision goes beyond Heisenberg sensitivity (i.e.  $\beta>2$ ), with few exceptions [22, 28, 29, 69–71]. Second, sensing weak fields with such probes is challenging as, for instance, critical points usually occur at finite field values and the precision quickly drops away from that point. Therefore, quantum probes that operate with super-Heisenberg precision for detecting weak fields are highly desirable.

The presence of a gradient field across a lattice makes the on-site energies off-resonant. Consequently, the tunneling rate is suppressed and the wave function of the particles localizes in space. This is known as Stark localization [72] and has been exploited for inducing single-particle [73–78] and many-body localization without disorder [78–95], probing the geometry of nano-structures [96], protecting many-body coherence from the environment [97], investigating gauge theories [98–

100] and creating quantum scars [48, 101–105]. Stark localization has been experimentally observed in ion-traps [106], ultracold atoms trapped in optical lattices [102, 107], and superconducting simulators [108]. For a one-dimensional single-particle system, the Stark localization takes place at infinitesimal fields in the limit of large lattice sizes [76]. This resembles Anderson localization [109], without disorder. One may wonder whether Stark localization transition can achieve enhanced precision sensing, in the same spirit as other forms of criticality [20–34]. In particular, it will be remarkable if Stark probes could reach super-Heisenberg precision. The key fact is that Stark localization transition takes place at the zero-field limit. Quantum-enhanced sensitivity in such a transition can be a breakthrough in ultra-precise sensing of weak fields, a domain that most many-body sensors fail. In addition, since Stark localization happens across the whole spectrum it provides more thermal robustness than conventional criticality which is limited to the ground state.

In this letter, we show that Stark probes can indeed achieve strong super-Heisenberg scaling, with  $\beta \approx 6$  for the ground state and  $\beta \approx 4$  for the mid-spectrum eigenstates, for weak-field sensing. Such quantum-enhanced precision can be obtained in the extended phase and stretches beyond the transition point. In the localized phase, the obtainable precision saturates to its thermodynamic limit as system size increases showing that one can emulate thermodynamic behavior using finite systems. Remarkably, a simple position measurement is enough to closely achieve the ultimate precision bound with super-Heisenberg scaling. In addition, through extensive finite-size scaling analysis, we determine several critical exponents and their relationships. Surprisingly, Stark probes can still operate at thermal equilibrium for which we have identified universal scaling behavior with respect to system size and temperature.

*Ultimate precision limit.*— Let's consider a quantum probe whose density matrix  $\rho(h)$  depends on an under scrutiny parameter  $h$ . To do so, one has to perform a measurement, described by a set of projective operators  $\{\Pi_i\}$ , on the probe. The result is described by a classical probability distribution in which each outcome appears with

the probability  $p_i(h)=\text{Tr}[\Pi_i\rho(h)]$ . For this measurement setup,  $\mathcal{F}$  in the Cramér-Rao inequality is called Classical Fisher Information (CFI),  $\mathcal{F}_C(h)=\sum_i p_i(h)(\partial_h \ln p_i(h))^2$  [110]. Optimizing the CFI over all possible measurement setups leads to Quantum Fisher Information (QFI), namely  $\mathcal{F}_Q(h)=\max_{\{\Pi_i\}} \mathcal{F}_C(h)$ , determining the ultimate precision limit achievable by a quantum probe [111]. A closed form for the QFI obtained through fidelity susceptibility  $\chi(h)$  [112] which for an incremental change in the parameter  $\Delta h \rightarrow 0$  can be approximated as  $\chi(h)=2(1-\tilde{F}(h))/\Delta h^2$ . Here,  $\tilde{F}(h)=\text{Tr} \sqrt{\rho(h)^{1/2}\rho(h+\Delta h)\rho(h)^{1/2}}$  is the fidelity between the two density matrices  $\rho(h)$  and  $\rho(h+\Delta h)$ . The QFI is then  $\mathcal{F}_Q(h)=4\chi(h)$ . This closed form exempts us from the notorious optimization over measurement setups.

*Model.*— We consider a one-dimensional probe with  $L$  sites in which one particle can tunnel to its neighbors with rate  $J$ . The probe is affected by a gradient field  $h$  which we would like to estimate. The Hamiltonian is

$$H(h) = J \sum_{i=1}^{L-1} (|i\rangle\langle i+1| + |i+1\rangle\langle i|) + h \sum_{i=1}^L |i\rangle\langle i|. \quad (1)$$

As  $h/J$  increases, the system goes through a phase transition from an extended phase to a Stark localized regime [76, 78, 79, 83, 84]. The transition is dramatic and affects the entire spectrum of the system which makes it very distinct from the conventional quantum phase transition as a property of the ground state [87]. While our study focuses on a single-particle system, generalization to multi-particle cases is straightforward. However, the results are expected to be different in the case of many-body interacting systems.

*Gradient field sensing.*— For our system in Eq. (1), in the thermodynamic limit (i.e.  $L \rightarrow \infty$ ), the localization transition for all energy levels takes place at  $h=h_c=0$  [76]. One can renormalize the energy of the system as  $\varepsilon=(E-E_{\min})/(E_{\max}-E_{\min})$ , with  $E_{\min}$  and  $E_{\max}$  as extremal eigenenergies of the Hamiltonian  $H(h)$  to fit the whole spectrum of the system within  $0 \leq \varepsilon \leq 1$ . For any given  $\varepsilon$ , the QFI with respect to  $h$  has been calculated for the closest eigenstate. In Figs. 1(a) and (b), we plot  $\mathcal{F}_Q$  as a function of  $h$  for various  $L$ , when our probe is in the ground state ( $\varepsilon = 0$ ) and a mid-spectrum eigenstate ( $\varepsilon = 0.5$ ), respectively. The QFI takes its maximum value at  $h=h_{\max}$ , which is expected to become the critical point, i.e.  $h_{\max}=h_c$ , in the thermodynamic limit. While for the ground state, see Fig.1(a), the maximum takes place at vanishingly small fields, namely  $h_{\max} \rightarrow 0$ , for the mid-spectrum, see Fig.1(b), a clear peak for the QFI can be observed at non-zero  $h_{\max}$ . Regardless of the energy levels, several features can be observed. First, by increasing  $L$ , the peak of the QFI, namely  $\mathcal{F}_Q(h_{\max})$ , dramatically enhances showing divergence in the thermodynamic limit. Second, the position of the peak gradually moves towards zero suggesting that in the thermodynamic limit one has  $h_{\max} \rightarrow h_c=0$ . Third, despite the decay of the QFI in the localized regime, its value remains high for a large interval of  $h$ , e.g. to have  $\mathcal{F}_Q \geq 10$ , the gradient field can be within the range  $0 \leq h/J \leq 0.25$  ( $0 \leq h \leq J$ )

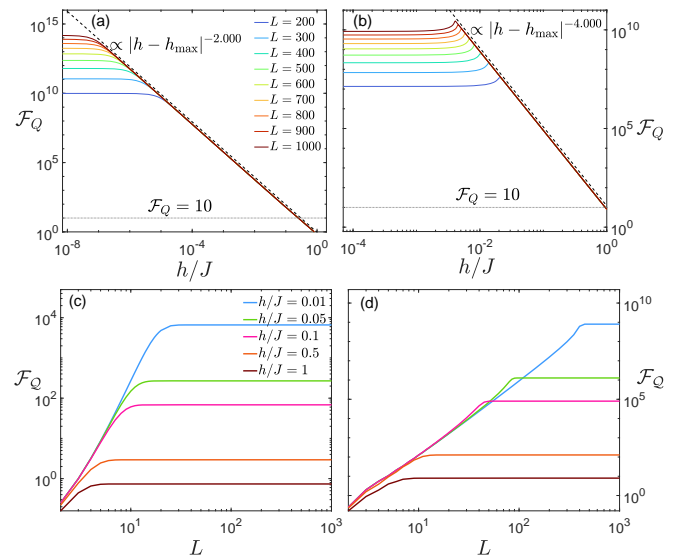


FIG. 1: The QFI as a function of Stark field  $h$  when our probe with different sizes  $L$  is prepared in (a) the ground state; and (b) the mid-spectrum eigenstate. The dashed lines in both panels are the best fit of  $\mathcal{F}_Q$  as a function of  $|h - h_{\max}|$  in the localized phase showing the behavior in the thermodynamic limit. In the localized phase, with various choices of  $h/J$ , the saturation of the QFI with respect to  $L$  is depicted for: (c) the ground state; and (d) the mid-spectrum state.

for the ground (mid-spectrum) state. Fourth, in the localized regime, after a certain threshold the QFI becomes size-independent showing divergence to the thermodynamic limit, represented by dashed lines in Figs.1(a) and (b). Finite-size effects are evident in the initial plateaus of the QFI, representing the extended phase of the system. Interestingly, the dashed lines suggest an algebraic behavior of the QFI, namely  $\mathcal{F}_Q(h) \propto |h - h_{\max}|^{-\alpha}$ , in the localized phase which can be perfectly fitted by  $\alpha=2.000$  for the ground state and  $\alpha=4.000$  for the mid-spectrum eigenstates. To see the convergence of the QFI in the localized phase, in Figs. 1(c) and (d) we plot  $\mathcal{F}_Q(h)$  as a function of system size  $L$  for various choices of  $h$  for the ground and the mid-spectrum eigenstates, respectively. By going away from the transition point  $h_{\max}$  the convergence becomes faster and QFI saturates to its thermodynamic value.

*Mobility edge.*— To see how Stark localization transition depends on energy, in Fig.2(a) we plot  $h_{\max}$  as a function of energy  $\varepsilon$  for various system sizes. The figure clearly indicates an energy-dependent transition which is known as mobility edge. In fact, mid-spectrum eigenstates are harder to localize than the eigenstates at the edges of the spectrum, a common feature that has also been observed in Anderson localization [113] and many-body [114] localization. As the system size increases, the mobility edge going to be disappeared. To see how  $h_{\max}$  decreases with increasing the system size at different energy scales, in Fig.2(b), we plot  $h_{\max}$  versus  $L$  for energies starting from the ground state ( $\varepsilon=0$ ) to mid-spectrum ( $\varepsilon=0.5$ ). Our numerical simulation (denoted by markers) is well described by a fitting function  $h_{\max}(L)=aL^{-b}$  (solid lines). The exponents

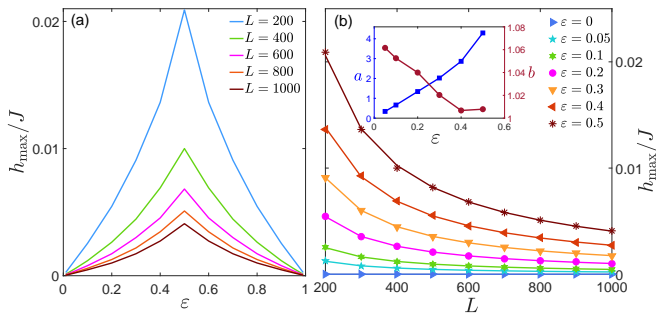


FIG. 2: (a) the transition point  $h_{\max}$  versus energy  $\varepsilon$ , in various system sizes, indicating the emergence of mobility edges in finite systems. (b) the scaling of  $h_{\max}/J$  with  $L$  for various  $\varepsilon$ . Markers and solid lines represent numerical results and fitting function  $h_{\max}=aL^{-b}$ , respectively. The inset provides  $a$  and  $b$  for different  $\varepsilon$ .

$a$  and  $b$  are plotted as a function of  $\varepsilon$  in the inset of Fig.2(b). While the exponent  $b$  shows a stable behavior around  $b \approx 1$ , the exponent  $a$  changes dramatically from  $a \approx 0$  (for the ground state) to  $a \approx 4$  (for the mid-spectrum).

*Super-Heisenberg sensitivity.*— In the extended phase, the QFI heavily depends on size  $L$ . To see how the QFI scales with the probe size, in Figs. 3(a) and (b), we plot the QFI at the transition point, i.e.  $\mathcal{F}_Q(h_{\max})$ , as a function of  $L$  for the ground ( $\varepsilon=0$ ) and the mid-spectrum ( $\varepsilon=0.5$ ) states, respectively. The QFIs are shown by markers and red lines are fitting functions  $\mathcal{F}_Q(h_{\max}) \propto L^\beta$  with  $\beta=5.980$  for the ground state and  $\beta=4.105$  for the mid-spectrum states. This shows strong super-Heisenberg scaling in which the exponent  $\beta$ , by our knowledge, exceeds all other known many-body probes with local interaction and bounded spectrum. We highlight

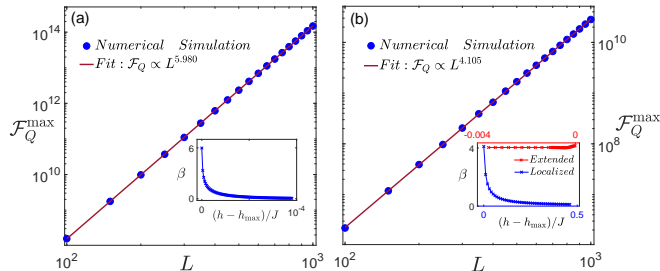


FIG. 3: The maximum of QFI (markers) as a function of  $L$  for (a) the ground state ( $\varepsilon=0$ ); and (b) the mid-spectrum eigenstate ( $\varepsilon=0.5$ ). The solid red lines are fitting of the form  $\mathcal{F}_Q^{\max}(h_{\max}) \propto L^\beta$  with  $\beta=5.980$  for  $\varepsilon=0$  and  $\beta=4.105$  for  $\varepsilon=0.5$ . The inset of each panel represents the behavior of  $\beta$  as  $h$  goes away from criticality. For the ground state (left panel)  $h_{\max}=0$ , the exponent is only shown in the localized phase. In the mid spectrum (right panel),  $\beta$  remains almost steady in the extended phase and drops in the localized phase

these as the main results of the letter. By entering the localized regime the exponent  $\beta$  is expected to go down to eventually become zero. This behavior of  $\beta$  is depicted in the insets of Figs. 3(a) and (b). In the mid spectrum, the exponent  $\beta$  remains steady in the extended phase which shows that

quantum-enhanced sensitivity can be achieved in the extended phase and stretches beyond the transition point.

*Finite-size scaling.*— While Figs.1(a) and (b) suggest the asymptotic behavior of  $\mathcal{F}_Q \propto |h - h_{\max}|^{-\alpha}$  (with  $h_{\max} \rightarrow h_c=0$ ) in  $L \rightarrow \infty$ , the finite-size analysis at the transition point  $h=h_{\max}$ , see Figs. 3(a) and (b), indicates  $\mathcal{F}_Q(h=h_{\max}) \propto L^\beta$ . These two behaviors can be merged in a single ansatz

$$\mathcal{F}_Q(h) \propto \frac{1}{L^{-\beta} + A|h - h_{\max}|^\alpha}, \quad (2)$$

where  $A$  is a constant. In the localized regime, where  $|h - h_{\max}|^\alpha \gg L^{-\beta}$ , the dependence of system size  $L$  becomes negligible. Thanks to the large value of  $\beta$  the convergence to this limit is very rapid in our Stark probe. The algebraic behavior of QFI hints that this transition might be of the second-order type. Any second-order phase transition is accompanied by the emergence of a diverging length scale as  $\xi \sim |h - h_c|^{-\nu}$ , where the exponent  $\nu$  controls the speed of divergence. In the case of localization transition,  $\xi$  is indeed the localization length. To verify the nature of the transition and determine the critical exponents, we consider a conventional second-order finite-size scaling analysis. This implies that the QFI follows ansatz

$$\mathcal{F}_Q(h) = L^{\alpha/\nu} g(L^{1/\nu}(h - h_c)), \quad (3)$$

where,  $g(\cdot)$  is an arbitrary function. To verify the above ansatz one can plot the rescaled QFI, namely  $L^{-\alpha/\nu} \mathcal{F}_Q(h)$ , versus  $L^{1/\nu}(h - h_c)$  for different system sizes. By tuning the parameter  $h_c$  and the exponents  $\alpha$  and  $\nu$  one tries to collapse all the curves of different system sizes on a single one. In Figs.4(a) and (b), we plot the best achievable data collapse, using Python package Pyfssa [115, 116], for probe sizes of lengths  $L=200$  to  $L=1000$  for  $\varepsilon=0$  and  $\varepsilon=0.5$ , respectively. Our careful finite-size scaling analysis results in  $(h_c, \alpha, \nu) = (4.37 \times 10^{-10}, 2.00, 0.33)$  and  $(h_c, \alpha, \nu) = (1.03 \times 10^{-5}, 4.00, 1.00)$ , for the ground and the mid-spectrum states, respectively. The values obtained for  $\alpha$  is fully consistent with the values extracted by independent data fitting in Figs. 1(a) and (b). In addition, the small values found for  $h_c$  are also in full agreement with the analysis of Figs. 2(a) and (b).

Note that the two ansatzes in Eq.(2) and Eq. (3) are both describing the QFI and thus cannot be independent. Indeed, by factorizing  $L^\beta$  from Eq.(2) one can easily show that the two ansatzes will be the same if and only if

$$\beta = \frac{\alpha}{\nu}. \quad (4)$$

This means that  $\alpha$ ,  $\beta$ , and  $\nu$  are not independent exponents and two of them can describe the Stark transition. In TABLE I we report the obtained values of  $\alpha$ ,  $\nu$ ,  $\alpha/\nu$  and  $\beta$  across the whole spectrum. Two important features can be observed: (i) the critical exponents found for the ground state are quite different from the ones obtained for other energies; and (ii) Eq. (4), remains valid with high accuracy across the whole spectrum, signaling the generality of our analysis.

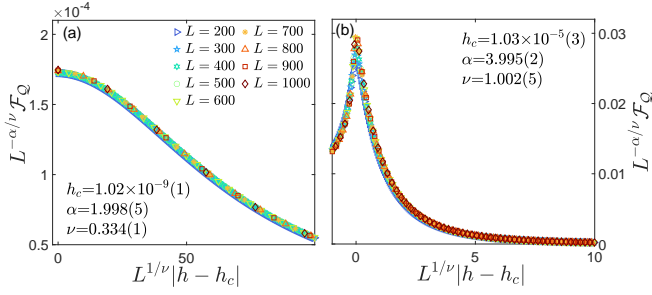


FIG. 4: Finite-size scaling analysis using Eq. (3) for (a) the ground state; and (b) the mid-spectrum eigenstate. The optimal data collapse is obtained for the reported  $(h_c, \alpha, \nu)$ .

$\varepsilon$	0	0.1	0.2	0.3	0.4	0.5
$\alpha$	1.998	3.746	3.898	3.971	3.995	3.995
$\nu$	0.334	0.944	0.979	0.996	1.002	1.002
$\alpha/\nu$	5.977	3.969	3.983	3.986	3.989	3.989
$\beta$	5.980	4.128	4.086	4.073	4.055	4.105

TABLE I: The exponents across the spectrum. The critical exponents  $\alpha$  and  $\nu$  are obtained from the finite-size scaling analysis in Fig. 4 and the exponent  $\beta$  is extracted from the data analysis in Fig. 3.

*Optimal measurement.*— Saturating the quantum Cramér-Rao bound, generally demands complex optimal measurements in a highly entangled basis which may even depend on the unknown parameter  $h$ . Therefore, finding a sub-optimal but experimentally feasible set of measurements whose precision can closely saturate the Cramér-Rao bound is highly desirable. Interestingly, in our Stark probe, a simple position measurement described by local projective operators  $\{\Pi_i = |i\rangle\langle i|\}_{i=1}^L$  can nearly saturate the QFI, for both the ground and the mid-spectrum states. In fact, the obtained CFI also reveals super-Heisenberg scaling with a corresponding exponent  $\beta$  very close to the one obtained from QFI (see the Supplementary Materials (SM)).

*Thermal probes.*— Apart from the ground state, which is reachable by cooling, accessing individual eigenstates is very difficult. In practice, our probe might be described by a thermal state  $\rho(h, T) = e^{-H/KT} / Z$ , where  $T$  is temperature,  $K$  is Boltzmann constant and  $Z = \text{Tr} [e^{-H/KT}]$  is the partition function. Note that, the QFI is still computed with respect to  $h$  and temperature is only a parameter. We consider two different scenarios with  $h$  being in the extended phase, namely  $h = 10^{-8}J$ , and in the localized phase, namely  $h = 0.05J$ . The QFI for both cases is plotted as a function of temperature in Figs. 5(a) and (b), respectively. The QFI starts with a plateau which extends over temperatures for which  $KT < \Delta E$ , where  $\Delta E = E_2 - E_1$  is the energy gap of the system. In this regime, the thermal state is described by the ground state and thus the behavior of the probe is as before. That is why in the extended phase, shown in Fig. 5(a), the plateaus are separated for each system size while in the localized phase, depicted in Fig. 5(b), they collapse on each other. Interesting behavior can be ob-

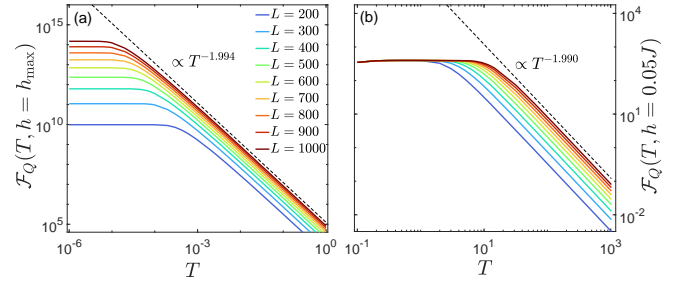


FIG. 5: The QFI of the thermal state as a function of temperature  $T$  for various system sizes, when the probe is operating at: (a) the transition point  $h = h_{\max} = 10^{-8}J$ ; and (b) the localized phase with  $h = 0.05J$ .

served for  $KT > \Delta E$ , where the QFI decays as temperature increases. In this regime, as shown in Fig. 5, for both localized and extended probes, the QFI decays as  $\mathcal{F}_Q \propto c(L)T^{-\mu}$ , where  $c(L)$  is a size-dependent constant and  $\mu = 1.99$  is a universal exponent. In the SM, it has been shown that  $c(L)$  scales algebraically with system size as  $c(L) \propto L^\gamma$ , with  $\gamma = 2.0$ . Therefore, for a general field  $h$  and in the limit of  $KT > \Delta E$  the QFI is described by a universal form as

$$\mathcal{F}_Q(h) \sim f(h)T^{-\mu}L^\gamma. \quad (5)$$

Notably, the value of QFI remains considerable for high temperatures, e.g. one has  $\mathcal{F}_Q \approx 10^5$  at  $T = 1$  for the extended phase and  $\mathcal{F}_Q \approx 10^2$  at  $T = 10$  for the localized phase.

*Conclusion.*— We have shown that single-particle Stark localization probes are extremely precise in measuring weak gradient fields, which are difficult to be detected by conventional probes. They can operate with strong super-Heisenberg precision over a region which stretches from the extended phase and goes beyond the transition point. As Stark localization takes place across the whole spectrum, the probe can be used in all energy scales. In the localized phase, namely large gradient field, the system converges to its thermodynamic behavior and QFI becomes size-independent. Through extensive finite-size scaling analysis across the whole spectrum, we have determined the critical exponents and their relationship at the vicinity of the Stark localization transition. We have also identified the universal behavior of the probe at thermal equilibrium with respect to size and temperature.

*Acknowledgment.*— A.B. acknowledges support from the National Key R&D Program of China (Grant No. 2018YFA0306703), the National Science Foundation of China (Grants No. 12050410253, No. 92065115, and No. 12274059), and the Ministry of Science and Technology of China (Grant No. QNJ2021167001L). R.Y. thanks the National Science Foundation of China for the International Young Scientists Fund (Grant No. 12250410242).

\* Electronic address: xjhe@std.uestc.edu.cn

† Electronic address: RozhinYousefjani@uestc.edu.cn

- ‡ Electronic address: abolfazl.bayat@uestc.edu.cn
- [1] C. R. Rao, in *Breakthroughs in statistics* (Springer, 1992), pp. 235–247.
- [2] S. L. Braunstein and C. M. Caves, *Phys. Rev. Lett.* **72**, 3439 (1994).
- [3] H. Cramér, *Mathematical methods of statistics*, vol. 43 (Princeton university press, 1999).
- [4] M. G. Paris, *Int. J. Quantum Inf.* **7**, 125 (2009).
- [5] C. L. Degen, F. Reinhard, and P. Cappellaro, *Rev. Mod. Phys.* **89**, 035002 (2017).
- [6] D. Braun, G. Adesso, F. Benatti, R. Floreanini, U. Marzolino, M. W. Mitchell, and S. Pirandola, *Rev. Mod. Phys.* **90**, 035006 (2018).
- [7] D. M. Greenberger, M. A. Horne, and A. Zeilinger, in *Bell's theorem, quantum theory and conceptions of the universe* (Springer, 1989), pp. 69–72.
- [8] V. Giovannetti, S. Lloyd, and L. Maccone, *Science* **306**, 1330 (2004).
- [9] D. Leibfried, M. D. Barrett, T. Schaetz, J. Britton, J. Chiaverini, W. M. Itano, J. D. Jost, C. Langer, and D. J. Wineland, *Science* **304**, 1476 (2004).
- [10] V. Giovannetti, S. Lloyd, and L. Maccone, *Phys. Rev. Lett.* **96**, 010401 (2006).
- [11] K. Banaszek, R. Demkowicz-Dobrzański, and I. A. Walmsley, *Nat. Photon.* **3**, 673 (2009).
- [12] V. Giovannetti, S. Lloyd, and L. Maccone, *Nat. Photon.* **5**, 222 (2011).
- [13] F. Fröwis and W. Dür, *Phys. Rev. Lett.* **106**, 110402 (2011).
- [14] R. Demkowicz-Dobrzański, J. Kołodyński, and M. Guţă, *Nat. Commun.* **3**, 1 (2012).
- [15] K. Wang, X. Wang, X. Zhan, Z. Bian, J. Li, B. C. Sanders, and P. Xue, *Phys. Rev. A* **97**, 042112 (2018).
- [16] H. Kwon, K. C. Tan, T. Volkoff, and H. Jeong, *Phys. Rev. Lett.* **122**, 040503 (2019).
- [17] M. Raghunandan, J. Wrachtrup, and H. Weimer, *Phys. Rev. Lett.* **120**, 150501 (2018).
- [18] T. L. Heugel, M. Biondi, O. Zilberberg, and R. Chitra, *Phys. Rev. Lett.* **123**, 173601 (2019).
- [19] L.-P. Yang and Z. Jacob, *Journal of Applied Physics* **126**, 174502 (2019).
- [20] P. Zanardi and N. Paunković, *Phys. Rev. E* **74**, 031123 (2006).
- [21] P. Zanardi, H. Quan, X. Wang, and C. Sun, *Phys. Rev. A* **75**, 032109 (2007).
- [22] S.-J. Gu, H.-M. Kwok, W.-Q. Ning, H.-Q. Lin, et al., *Phys. Rev. B* **77**, 245109 (2008).
- [23] P. Zanardi, M. G. Paris, and L. C. Venuti, *Phys. Rev. A* **78**, 042105 (2008).
- [24] C. Invernizzi, M. Korbman, L. C. Venuti, and M. G. Paris, *Phys. Rev. A* **78**, 042106 (2008).
- [25] S.-J. Gu, *Int. J. Mod. Phys. B* **24**, 4371 (2010).
- [26] S. Gammelmark and K. Mølmer, *New J. Phys.* **13**, 053035 (2011).
- [27] M. Skotiniotis, P. Sekatski, and W. Dür, *New J. Phys.* **17**, 073032 (2015).
- [28] M. M. Rams, P. Sierant, O. Dutta, P. Horodecki, and J. Zakrzewski, *Phys. Rev. X* **8**, 021022 (2018).
- [29] B.-B. Wei, *Phys. Rev. A* **99**, 042117 (2019).
- [30] Y. Chu, S. Zhang, B. Yu, and J. Cai, *Phys. Rev. Lett.* **126**, 010502 (2021).
- [31] R. Liu, Y. Chen, M. Jiang, X. Yang, Z. Wu, Y. Li, H. Yuan, X. Peng, and J. Du, *npj Quantum Information* **7**, 1 (2021).
- [32] V. Montenegro, U. Mishra, and A. Bayat, *Phys. Rev. Lett.* **126**, 200501 (2021).
- [33] S. S. Mirkhalaf, D. B. Orenes, M. W. Mitchell, and E. Witkowska, *Phys. Rev. A* **103**, 023317 (2021).
- [34] R. Di Candia, F. Minganti, K. Petrovnin, G. Paraoanu, and S. Felicetti, arXiv:2107.04503 (2021).
- [35] K. Baumann, C. Guerlin, F. Brennecke, and T. Esslinger, *Nature* **464**, 1301 (2010).
- [36] M. P. Baden, K. J. Arnold, A. L. Grimsmo, S. Parkins, and M. D. Barrett, *Phys. Rev. Lett.* **113**, 020408 (2014).
- [37] J. Klinder, H. Keßler, M. Wolke, L. Mathey, and A. Hemmerich, *Proceedings of the National Academy of Sciences* **112**, 3290 (2015).
- [38] S. Rodriguez, W. Casteels, F. Storme, N. C. Zambon, I. Sagnes, L. Le Gratiet, E. Galopin, A. Lemaître, A. Amo, C. Ciuti, et al., *Phys. Rev. Lett.* **118**, 247402 (2017).
- [39] M. Fitzpatrick, N. M. Sundaresan, A. C. Li, J. Koch, and A. A. Houck, *Phys. Rev. X* **7**, 011016 (2017).
- [40] J. M. Fink, A. Dombi, A. Vukics, A. Wallraff, and P. Domokos, *Phys. Rev. X* **7**, 011012 (2017).
- [41] T. Ilias, D. Yang, S. F. Huelga, and M. B. Plenio, *PRX Quantum* **3**, 010354 (2022).
- [42] V. Montenegro, M. Genoni, A. Bayat, and M. Paris, arXiv:2301.02103 (2023).
- [43] J. C. Budich and E. J. Bergholtz, *Phys. Rev. Lett.* **125**, 180403 (2020).
- [44] S. Sarkar, C. Mukhopadhyay, A. Alase, and A. Bayat, *Phys. Rev. Lett.* **129**, 090503 (2022).
- [45] F. Koch and J. C. Budich, *Phys. Rev. Res.* **4**, 013113 (2022).
- [46] M. Yu, X. Li, Y. Chu, B. Mera, F. N. Ünal, P. Yang, Y. Liu, N. Goldman, and J. Cai, arXiv:2206.00546 (2022).
- [47] S. Dooley, *PRX Quantum* **2**, 020330 (2021).
- [48] J.-Y. Desaulles, A. Hudomal, C. J. Turner, and Z. Papić, *Phys. Rev. Lett.* **126**, 210601 (2021).
- [49] A. Yoshinaga, Y. Matsuzaki, and R. Hamazaki, arXiv:2211.09567 (2022).
- [50] S. Dooley, S. Pappalardi, and J. Goold, *Phys. Rev. B* **107**, 035123 (2023).
- [51] U. Mishra and A. Bayat, *Phys. Rev. Lett.* **127**, 080504 (2021).
- [52] U. Mishra and A. Bayat, *Sci. Rep.* **12**, 1 (2022).
- [53] H. M. Wiseman, *Phys. Rev. Lett.* **75**, 4587 (1995).
- [54] M. A. Armen, J. K. Au, J. K. Stockton, A. C. Doherty, and H. Mabuchi, *Phys. Rev. Lett.* **89**, 133602 (2002).
- [55] A. Fujiwara, *J. Phys. A Math. Gen.* **39**, 12489 (2006).
- [56] B. L. Higgins, D. W. Berry, S. D. Bartlett, H. M. Wiseman, and G. J. Pryde, *Nature* **450**, 393 (2007).
- [57] D. W. Berry, B. L. Higgins, S. D. Bartlett, M. W. Mitchell, G. J. Pryde, and H. M. Wiseman, *Phys. Rev. A* **80**, 052114 (2009).
- [58] R. Said, D. Berry, and J. Twamley, *Phys. Rev. B* **83**, 125410 (2011).
- [59] R. Okamoto, M. Iefuji, S. Oyama, K. Yamagata, H. Imai, A. Fujiwara, and S. Takeuchi, *Phys. Rev. Lett.* **109**, 130404 (2012).
- [60] C. Bonato, M. S. Blok, H. T. Dinani, D. W. Berry, M. L. Markham, D. J. Twitchen, and R. Hanson, *Nat. Nanotechnol.* **11**, 247 (2016).
- [61] R. Okamoto, S. Oyama, K. Yamagata, A. Fujiwara, and S. Takeuchi, *Phys. Rev. A* **96**, 022124 (2017).
- [62] S. Fernández-Lorenzo and D. Porras, *Phys. Rev. A* **96**, 013817 (2017).
- [63] S. Gammelmark and K. Mølmer, *Phys. Rev. Lett.* **112**, 170401 (2014).
- [64] F. Albarelli, M. A. Rossi, M. G. Paris, and M. G. Genoni, *New J. Phys.* **19**, 123011 (2017).
- [65] M. A. Rossi, F. Albarelli, D. Tamascelli, and M. G. Genoni, *Phys. Rev. Lett.* **125**, 200505 (2020).

- [66] D. Yang, S. F. Huelga, and M. B. Plenio, arXiv:2209.08777 (2022).
- [67] D. Burgarth, V. Giovannetti, A. N. Kato, and K. Yuasa, *New J. Phys.* **17**, 113055 (2015).
- [68] V. Montenegro, G. S. Jones, S. Bose, and A. Bayat, *Phys. Rev. Lett.* **129**, 120503 (2022).
- [69] S. Boixo, S. T. Flammia, C. M. Caves, and J. M. Geremia, *Phys. Rev. Lett.* **98**, 090401 (2007).
- [70] S. Roy and S. L. Braunstein, *Phys. Rev. Lett.* **100**, 220501 (2008).
- [71] M. Beau and A. del Campo, *Phys. Rev. Lett.* **119**, 010403 (2017).
- [72] G. H. Wannier, *Phys. Rev.* **117**, 432 (1960).
- [73] H. Fukuyama, R. A. Bari, and H. C. Fogedby, *Phys. Rev. B* **8**, 5579 (1973).
- [74] M. Holthaus, G. Ristow, and D. Hone, *EPL* **32**, 241 (1995).
- [75] A. Kolovsky and H. Korsch, *Phys. Rev. A* **67**, 063601 (2003).
- [76] A. R. Kolovsky, *Phys. Rev. Lett.* **101**, 190602 (2008).
- [77] A. R. Kolovsky and E. N. Bulgakov, *Phys. Rev. A* **87**, 033602 (2013).
- [78] E. van Nieuwenburg, Y. Baum, and G. Refael, *Proc. Natl. Acad. Sci. U.S.A.* **116**, 9269 (2019).
- [79] M. Schulz, C. Hooley, R. Moessner, and F. Pollmann, *Phys. Rev. Lett.* **122**, 040606 (2019).
- [80] L.-N. Wu and A. Eckardt, *Phys. Rev. Lett.* **123**, 030602 (2019).
- [81] D. S. Bhakuni, R. Nehra, and A. Sharma, *Phys. Rev. B* **102**, 024201 (2020).
- [82] D. S. Bhakuni and A. Sharma, *Phys. Rev. B* **102**, 085133 (2020).
- [83] R. Yao and J. Zakrzewski, *Phys. Rev. B* **102**, 104203 (2020).
- [84] T. Chanda, R. Yao, and J. Zakrzewski, *Phys. Rev. Res.* **2**, 032039 (2020).
- [85] S. R. Taylor, M. Schulz, F. Pollmann, and R. Moessner, *Phys. Rev. B* **102**, 054206 (2020).
- [86] Y.-Y. Wang, Z.-H. Sun, and H. Fan, *Phys. Rev. B* **104**, 205122 (2021).
- [87] L. Zhang, Y. Ke, W. Liu, and C. Lee, *Phys. Rev. A* **103**, 023323 (2021).
- [88] Q. Guo, C. Cheng, H. Li, S. Xu, P. Zhang, Z. Wang, C. Song, W. Liu, W. Ren, H. Dong, et al., *Phys. Rev. Lett.* **127**, 240502 (2021).
- [89] R. Yao, T. Chanda, and J. Zakrzewski, *Phys. Rev. B* **104**, 014201 (2021).
- [90] E. V. Doggen, I. V. Gornyi, and D. G. Polyakov, *Phys. Rev. B* **105**, 134204 (2022).
- [91] G. Zisling, D. M. Kennes, and Y. B. Lev, *Phys. Rev. B* **105**, L140201 (2022).
- [92] A. L. Burin, *Phys. Rev. B* **105**, 184206 (2022).
- [93] C. Bertoni, J. Eisert, A. Kshetrimayum, A. Nietner, and S. Thomson, arXiv:2208.14432 (2022).
- [94] I. Lukin, Y. V. Slyusarenko, and A. Sotnikov, *Phys. Rev. B* **105**, 184307 (2022).
- [95] E. Vernek, *Phys. Rev. B* **105**, 075124 (2022).
- [96] T. Pedersen, H. Cornean, D. Krejčířik, N. Raymond, and E. Stockmeyer, *New J. Phys.* **24**, 093005 (2022).
- [97] S. Sarkar and B. Buca, arXiv:2204.13354 (2022).
- [98] B. Yang, H. Sun, R. Ott, H.-Y. Wang, T. V. Zache, J. C. Halimeh, Z.-S. Yuan, P. Hauke, and J.-W. Pan, *Nature* **587**, 392 (2020).
- [99] J. C. Halimeh, H. Lang, J. Mildenerberger, Z. Jiang, and P. Hauke, *PRX Quantum* **2**, 040311 (2021).
- [100] Z.-Y. Zhou, G.-X. Su, J. C. Halimeh, R. Ott, H. Sun, P. Hauke, B. Yang, Z.-S. Yuan, J. Berges, and J.-W. Pan, *Science* **377**, 311 (2022).
- [101] V. Khemani, M. Hermele, and R. Nandkishore, *Phys. Rev. B* **101**, 174204 (2020).
- [102] T. Kohlert, S. Scherg, P. Sala, F. Pollmann, B. H. Madhusudhana, I. Bloch, and M. Aidelsburger, arXiv:2106.15586 (2021).
- [103] S. Scherg, T. Kohlert, P. Sala, F. Pollmann, B. Hebbe Madhusudhana, I. Bloch, and M. Aidelsburger, *Nat. Commun.* **12**, 1 (2021).
- [104] E. V. Doggen, I. V. Gornyi, and D. G. Polyakov, *Phys. Rev. B* **103**, L100202 (2021).
- [105] G.-X. Su, H. Sun, A. Hudomal, J.-Y. Desaulles, Z.-Y. Zhou, B. Yang, J. C. Halimeh, Z.-S. Yuan, Z. Papić, and J.-W. Pan, arXiv:2201.00821 (2022).
- [106] W. Morong, F. Liu, P. Becker, K. Collins, L. Feng, A. Kyprianidis, G. Pagano, T. You, A. Gorshkov, and C. Monroe, *Nature* **599**, 393 (2021).
- [107] P. M. Preiss, R. Ma, M. E. Tai, A. Lukin, M. Rispoli, P. Zupancic, Y. Lahini, R. Islam, and M. Greiner, *Science* **347**, 1229 (2015).
- [108] A. H. Karamlou, J. Braumüller, Y. Yanay, A. Di Paolo, P. M. Harrington, B. Kannan, D. Kim, M. Kjaergaard, A. Melville, S. Muschinske, et al., *Npj Quantum Inf.* **8**, 1 (2022).
- [109] P. W. Anderson, *Phys. Rev.* **109**, 1492 (1958).
- [110] R. A. Fisher, *Philos. Trans. Royal Soc.* **222**, 309 (1922).
- [111] J. J. Meyer, *Quantum* **5**, 539 (2021).
- [112] W.-L. You, Y.-W. Li, and S.-J. Gu, *Phys. Rev. E* **76**, 022101 (2007).
- [113] D. Bruns, R. Haenel, and G. Tom, *J. Phys. Condens.* (2019).
- [114] D. J. Luitz, N. Laflorencie, and F. Alet, *Phys. Rev. B* **91**, 081103 (2015).
- [115] A. Sorge, *pyfssa 0.7.6* (2015), URL <https://doi.org/10.5281/zenodo.35293>.
- [116] O. Melchert, arXiv:0910.5403 (2009).

## Supplementary Materials

### ACCESSIBILITY OF SUPER-HEISENBERG SCALING

In the main text of the letter, we present a simple position measurement described by local projective operators as  $\{\Pi_i=|i\rangle\langle i|\}_{i=1}^L$  to nearly saturate the quantum Cramér-Rao bound. This section deals with providing numerical evidence for this claim. For  $p_i(h)=\text{Tr}[\Pi_i\rho(h)]$  as the probability of finding the particle in site  $i$ , the CFI can be calculated using  $\mathcal{F}_C(h)=\sum_i p_i(h)(\partial_h \ln p_i(h))^2$ . In Figs. S1 (a) and (b),  $\mathcal{F}_Q$  (markers) and  $\mathcal{F}_C$  (solid line) as a function of the gradient field  $h/J$  are plotted for two different probe sizes prepared in the ground state and mid-spectrum eigenstate, respectively. Surprisingly, the CFI obtained via position measurement highly resembles that of QFI for both scenarios. The maximum (peak) of CFI happens in the same  $h_{\max}$  for the QFI and by increasing the system size from  $L=200$  to  $L=1000$  smoothly skews toward vanishingly smaller values of  $h$ . This signals that in the thermodynamic limit (i.e.  $L\rightarrow\infty$ ) one has  $h_{\max}=h_c$  for both lowest and mid-spectrum energy levels. Similar to the QFI, the maximum of the CFI significantly increases, signaling the divergence of the CFI in the thermodynamic limit. The divergent and size-independent behaviors of the CFI in both extended and localized regimes hint that analog to the QFI, the thermodynamic behavior of the system far from criticality can be emulated by finite-size systems that are measured by  $\{\Pi_i=|i\rangle\langle i|\}_{i=1}^L$ . This is a powerful witness of closely saturating the quantum Cramér-Rao bound.

To capture the scaling behavior of the CFI with respect to probe size  $L$ , in Figs. S1 (c) and (d) we plot  $\mathcal{F}_C^{\max}(h_{\max})$  (solid line) as well as  $\mathcal{F}_Q^{\max}(h_{\max})$  (marker) for both lowest and mid-spectrum energy levels, respectively. Obviously, the CFI follows the QFI scaling behavior which can be described by  $\mathcal{F}_C^{\max}(h_{\max})\propto L^\beta$ . We found that for the ground state, the scaling exponent  $\beta$  of CFI converges to that of QFI. While for the mid-spectrum state, both the value and the scaling exponent  $\beta$  of QFI are quite close to those of CFI. This numerical simulation shows that the simple position measurement in our Stark probe is the optimal measurement setup that can saturate the quantum Cramér-Rao bound and achieve super-Heisenberg scaling.

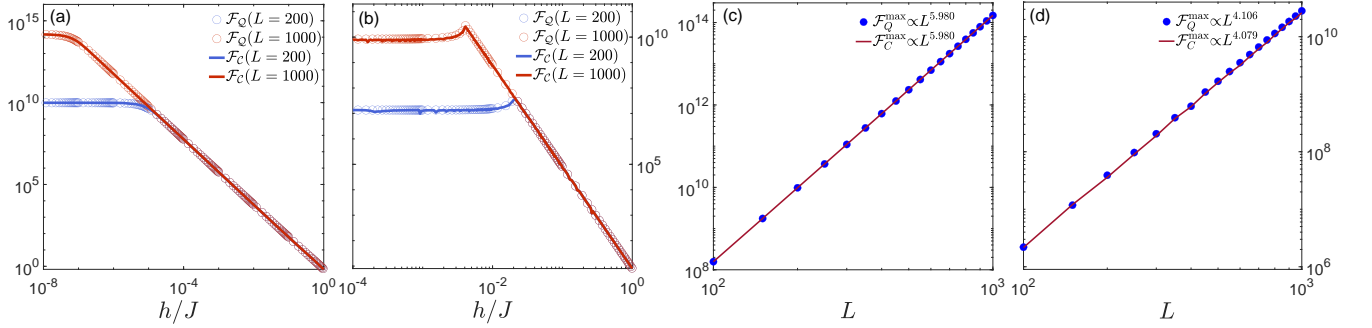


FIG. S1: The CFI and QFI as a function of Stark field  $h$  when our probe with system sizes  $L=200, 1000$  is prepared in (a) the ground state and (b) the mid-spectrum state. The maximum of QFI (markers) CFI (solid lines) as a function of system size  $L$  for (c) the ground state and (d) the mid-spectrum state. The optimal data fitting for numerical results of CFI is obtained as  $\mathcal{F}_C^{\max}(h_{\max})\propto L^\beta$  with  $\beta=5.980$  and  $\beta=4.079$  evaluated for the lowest and mid-spectrum energy levels, respectively.

### ALGEBRAIC BEHAVIOR OF THERMAL PROBE WHEN $KT>\Delta E$

Followed by our discussion in the main text about the performance of Stark probe in higher temperatures, in this section we present numerical evidence to prove the universal behavior  $\mathcal{F}_Q(h)\propto f(h)T^{-\mu}L^\gamma$  with  $f(h)$  as a non-zero constant. In Figs. S2 (a) and (b), the scaling behavior of the QFI with respect to probe size  $L$  in different temperatures  $T$  has been plotted for two scenarios. In panel (a) the Stark probe operates in its critical regime (i.e.  $h=h_{\max}$ ). In contrast, in panel (b), the gradient field is considered large enough ( $h=0.05J$ ) to assess the functionality of the probe in its off-critical regime. Clearly, for both scenarios, increasing the temperature reduces the QFI. The universal scaling behavior of the QFI with respect to probe size can be obtained by establishing a finite-size scaling analysis. In Figs. S2 (c) and (d), we plot the rescaled QFI (i.e.  $T^\mu\mathcal{F}_Q$ ) with respect to  $L$  for critical ( $h=h_{\max}$ ) and off-critical ( $h=0.05J$ ) regimes, respectively. For both scenarios, the best data collapse is obtained for  $T^\mu\mathcal{F}_Q\propto L^\gamma$  with  $\gamma=2.022$  and  $\gamma=2.001$  for the critical and off-critical regimes. This numerical simulation guarantees the validity of the universal behavior of thermal probe as  $\mathcal{F}_Q\propto T^{-2}L^2$ . Obviously, followed by the super-Heisenberg scaling with the ground state for  $KT<\Delta E$  at  $T\rightarrow 0$ , the Heisenberg precision can still be reachable for our Stark probe in a higher temperature and localized regime.

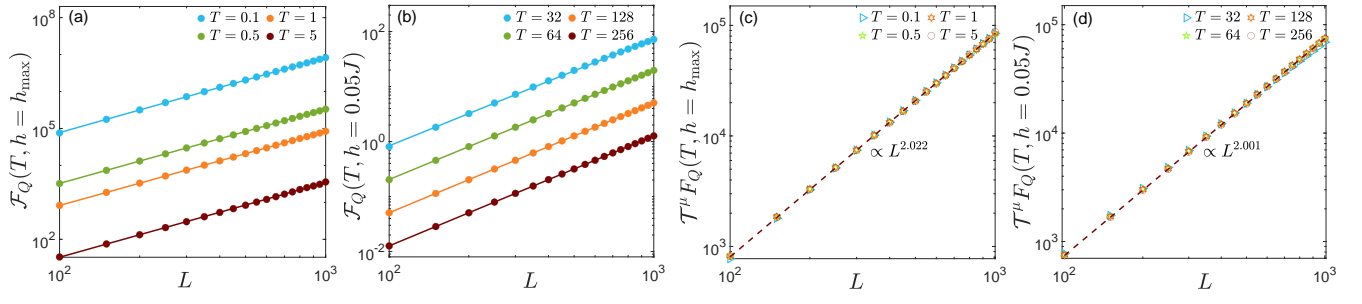


FIG. S2: The scaling behavior of QFI when  $KT > \Delta E$  and the Stark probe operate in its (a) critical and (b) off-critical (localized) regimes. The rescaled QFI as a function of  $L$  in (c) critical and (d) off-critical regimes. The best data collapse is obtained for  $T^\mu \mathcal{F}_Q \propto L^\gamma$  with  $\gamma$  as reported in the corresponding panel.